

Quasi-two-dimensional hole ordering and dimerized state in the CuO₂-chain layers in Sr₁₄Cu₂₄O₄₁

M. Matsuda

The Institute of Physical and Chemical Research (RIKEN), Wako, Saitama 351-0198, Japan

T. Yosihama and K. Kakurai

Neutron Scattering Laboratory, ISSP, University of Tokyo, Tokai, Ibaraki 319-1106, Japan

G. Shirane

Physics Department, Brookhaven National Laboratory, Upton, New York 11973

(Received 3 August 1998)

Neutron-scattering experiments have been performed on Sr₁₄Cu₂₄O₄₁ that consists of both chains and ladders of copper ions. We observed that the magnetic excitations from the CuO₂ chain have two branches and that both branches are weakly dispersive along the *a* and *c* axes. The ω -*Q* dispersion relation as well as the intensities can be reasonably described by a random-phase approximation with intradimer coupling $J = 11$ meV, interdimer coupling along the *c* axis $J_c = 0.75$ meV, and interdimer coupling along the *a* axis $J_a = 0.75$ meV. The dimer configuration indicates a quasi-two-dimensional hole ordering, resulting in an ordering of magnetic Cu²⁺ with spin- $\frac{1}{2}$ and nonmagnetic Cu, which forms the Zhang-Rice singlet. We have also studied the effect of Ca substitution for Sr on the dimer and the hole ordering. [S0163-1829(99)11401-2]

I. INTRODUCTION

Sr₁₄Cu₂₄O₄₁ consists of both two-leg ladders of copper ions and simple CuO₂ chains^{1,2} as shown in Fig. 1. Numerous experiments showed that the two-leg ladder has an excitation gap of ~ 35 meV,³⁻⁷ which is expected theoretically.⁸ An important feature of this compound is that stoichiometric Sr₁₄Cu₂₄O₄₁ contains hole carriers. It has been reported that most of the holes are localized in the chain and some exist in the ladder.⁹⁻¹¹ When Sr²⁺ sites are substituted by Ca²⁺ ions, the total number of the holes in the sample is unchanged but holes in the chain are transferred from the chain to the ladder^{10,11} and the system shows an insulator-to-metal transition.^{9,12} Superconductivity was also observed in Sr_{0.4}Ca_{13.6}Cu₂₄O₄₁ below $T_c = 10$ K under a high pressure of 3 GPa.¹³

In this paper we are only concerned with the magnetic properties in the chains. Figure 1(a) shows the CuO₂ chains in this compound. The copper ions are coupled by an almost 90° Cu-O-Cu bond along the *c* axis. Each chain is well isolated from each other along the *a* and *b* axes. As mentioned above, there are localized holes in the chain. It is expected that the hole spins are localized at oxygen¹⁰ and couple with copper spins to form the Zhang-Rice (ZR) singlet.¹⁴ The nonmagnetic Cu sites play an important role to form a dimerized state in the chain. First, the dimer is formed between Cu²⁺ spins that are separated by twice the distance between nearest-neighbor Cu ions along the *c* axis. The exchange interaction (~ 10 meV) is mediated via a nonmagnetic ZR singlet.^{5,15,16} Then the question is how the dimers are arranged and interact with each other. Matsuda *et al.*¹⁵ interpreted that each dimer is separated by one ZR singlet along the *c* axis (model I) as shown in Fig. 1(c). They also interpreted that the excitations at low *Q* ($L_{chain} < 0.4$) origi-

nate from a dimerized state in the chain and those at high *Q* ($L_{chain} > 0.6$) from a dimerized state due to the interladder coupling since two branches were observed for the gap excitations at low *Q* but only one branch at high *Q*.

NMR studies revealed the microscopic properties of the dimerized state.^{5,17} It was reported that both magnetic Cu²⁺ and a nonmagnetic ZR singlet exist in the chain. It was also found that an NMR peak originating from a ZR singlet gradually splits into two peaks below ~ 200 K. The results were discussed with two dimer models. One is model I mentioned above. This model was supported by Cox *et al.* by their x-ray measurements.¹⁸ In another model the dimers are separated by two nonmagnetic ZR singlets along the *c* axis (model II) as shown in Fig. 1(d). This model is consistent with the results of the electron-diffraction study by Hiroi *et al.*¹⁹ in which the CuO₂ chains show a modulated structure with a five times larger unit cell along the *c* axis in stoichiometric Sr₁₄Cu₂₄O₄₁. However, neither model can completely explain the NMR results.

Recently, two papers^{16,20} on neutron-scattering experiments came to our attention. Eccleston *et al.*¹⁶ explained the modulation of the excitations and intensities along the *c* axis convincingly by a simple model of an alternating chain with weak interdimer coupling²¹ ($J_2/J_1 \sim -0.1$, where J_1 and J_2 are intradimer and interdimer coupling, respectively), which is equivalent to model II. It is noted that two parallel branches along the *c* axis are not separated in the experiments because of insufficient resolution. Regnault *et al.*²⁰ briefly reported the measurement of two parallel branches in a wide range of *Q* ($0.05 \leq L_{chain} \leq 0.925$) along the *c* axis, which suggested a weak coupling along the *a* direction. The specific coupling along the *a* direction was recently reported by Cox *et al.*¹⁸ in their synchrotron x-ray study of the charge ordering at low temperatures.

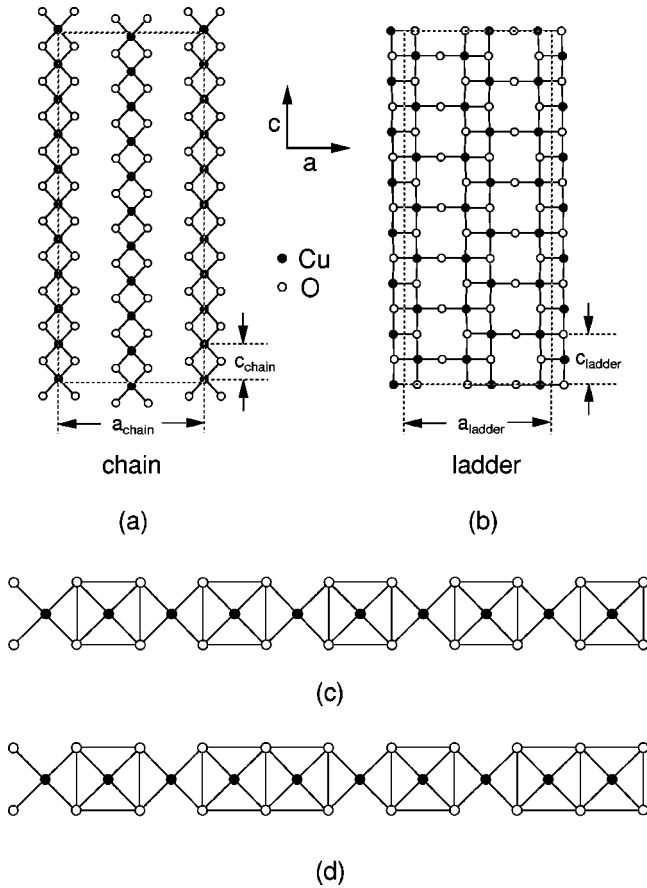


FIG. 1. Structure of the Cu_2O_2 chains (a) and the Cu_2O_3 ladders (b) in $\text{Sr}_{14}\text{Cu}_{24}\text{O}_{41}$. The lower part of the figure shows two dimer models as described in Sec. I: (c) model I and (d) model II. The squares denote Zhang-Rice singlet sites. Figure from Ref. 18.

Since dimerized states sometimes occur in spin (S) $\frac{1}{2}$ one-dimensional Heisenberg antiferromagnets such as the spin-Peierls state, it is quite natural to assume that the dimerized state in the chain of $\text{Sr}_{14}\text{Cu}_{24}\text{O}_{41}$ is also caused by a quantum effect in an $S = \frac{1}{2}$ one-dimensional Heisenberg antiferromagnet. On the other hand, almost isolated magnetic dimers were found in $\text{CaCuGe}_2\text{O}_6$ (Refs. 22 and 23) even though the geometrical arrangement of the magnetic moments seems three dimensional. It was also claimed that magnetic moments which are geometrically closest does not necessarily couple most dominantly in $\text{VODPO}_4 \cdot \frac{1}{2}\text{D}_2\text{O}$ (Ref. 24) and $(\text{VO})_2\text{P}_2\text{O}_7$ (Ref. 25) because of the strong superexchange pathways through a covalently bonded PO_4 group. These results suggest that unexpected pathways could become important in order to completely understand the magnetic properties of magnetic materials.

We have searched for a simple model of dimers with weak couplings along both c and a directions.²⁶ Somewhat surprisingly, a specific combination of the two couplings, as described by Leuenberger *et al.*²⁷ for $\text{Cs}_3\text{Cr}_2\text{Br}_9$, produces simple and elegant neutron-scattering cross sections that describe properly the measured dispersion and intensities. In this paper, we have studied the ω - Q dispersion relation perpendicular to the chain direction in considerable detail. By applying a random-phase approximation (RPA) treatment, we found that the interdimer coupling along the a axis (J_a

$= 0.75$ meV) is also important²⁸ as well as the interdimer coupling along the c axis ($J_c = 0.75$ meV). The model cross section will be given after the experimental data are presented. The dimer arrangement along the c axis is well described with model II. The dimer configuration we found in this study indicates a quasi-two-dimensional hole ordering, resulting in an ordering of Cu^{2+} and a ZR singlet in the ac plane. Ca substitution for Sr makes the magnetic excitation peaks broader as in the case of Y substitution²⁹ probably because the hole ordering is very sensitive to the hole number and the long-range dimer formation becomes disturbed.

II. EXPERIMENTAL DETAILS

The single crystals of $\text{Sr}_{14-x}\text{Ca}_x\text{Cu}_{24}\text{O}_{41}$ ($x=0$ and 3) were grown using a traveling solvent floating zone method at 3 bars oxygen atmosphere. The dimension of the cylindrically shaped crystals is about $5 \times 5 \times 30$ mm³. The effective mosaic of the single crystal is less than 0.4° with the spectrometer condition as described below. The $\text{Sr}_{14}\text{Cu}_{24}\text{O}_{41}$ crystal is the same one as used in Ref. 15. It is expected that Sr and Ca are distributed homogeneously in $\text{Sr}_{11}\text{Ca}_3\text{Cu}_{24}\text{O}_{41}$ since the lattice constants systematically change and the line-width of the nuclear Bragg peaks does not change when the ratio of Sr and Ca is changed. The lattice constants of $\text{Sr}_{14}\text{Cu}_{24}\text{O}_{41}$ and $\text{Sr}_{11}\text{Ca}_3\text{Cu}_{24}\text{O}_{41}$ are $a = 11.472$ Å and $c = 27.551$ Å and $a = 11.430$ Å and $c = 27.487$ Å at 15 K, respectively. The lattice constants are consistent with those obtained with powder samples.⁹

The neutron-scattering experiments were carried out on the ISSP-PONTA spectrometer installed at the 5G beam hole of the Japan Research Reactor 3M (JRR-3M) at the Japan Atomic Energy Research Institute (JAERI). The horizontal collimator sequences were $40' - 40' - S - 80' - 80'$. The final neutron energy was fixed at $E_f = 14.7$ meV. Pyrolytic graphite (002) was used as monochromator and analyzer. Contamination from higher-order beam was effectively eliminated using pyrolytic graphite filters after the sample. The single crystals were mounted in a closed cycle refrigerator and were oriented in the $(h, 0, l)$ scattering plane. As described in Ref. 1, there are three different values for the lattice constant c ($c_{\text{universal}} = 10 \times c_{\text{chain}} = 7 \times c_{\text{ladder}}$). Since we will show the magnetic and structural properties in the chain, c_{chain} will be used to express Miller indices.

III. EXPERIMENTAL RESULTS

A. Magnetic excitations from $\text{Sr}_{14}\text{Cu}_{24}\text{O}_{41}$ chain

1. Low-temperature dispersion

Figure 2 shows the typical neutron inelastic spectra at $(H, 0, L)$ in $\text{Sr}_{14}\text{Cu}_{24}\text{O}_{41}$ measured at 15 K. One or two distinct excitation peaks are observed in the $(H, 0, L)$ scattering plane as in the $(0, K, L)$ scattering plane that was previously reported in Refs. 15 and 29. The solid lines at $(2, 0, -0.20)$, $(2.75, 0, -0.20)$, $(2, 0, -0.75)$, and $(3, 0, -0.75)$ are fits to two Gaussians and those at $(2, 0, -0.70)$ and $(2.75, 0, -0.70)$ are the fits to a single Gaussian. The excitation peak positions are changed when H or L is changed, meaning a dispersion along the a and c axes. The width of the excitation peaks varies at different Q positions purely due

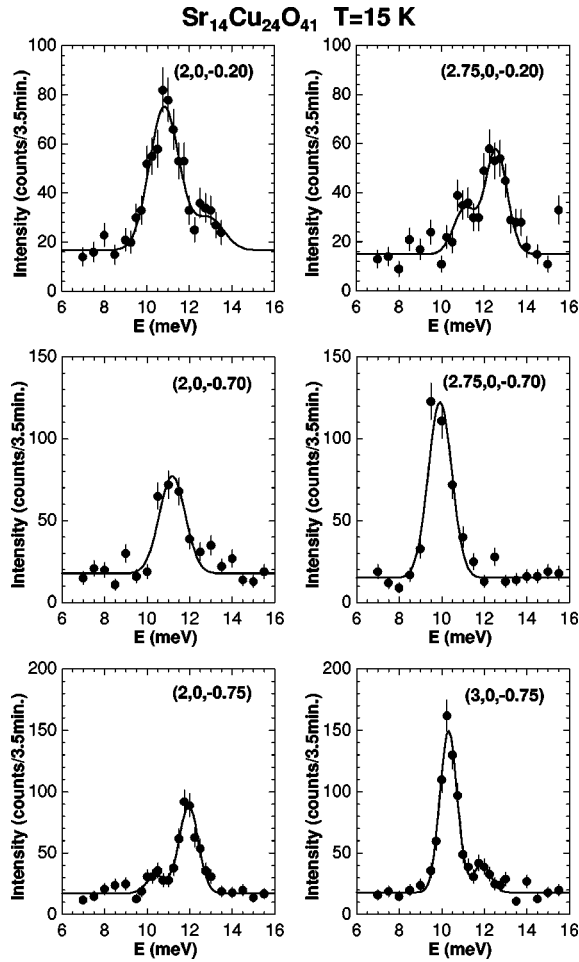


FIG. 2. Typical inelastic neutron spectra at $(H,0,L)$ at 15 K in $\text{Sr}_{14}\text{Cu}_{24}\text{O}_{41}$. The solid lines are the results of fits to a single Gaussian or two Gaussians.

to the resolution focusing effect. At $(3,0,-0.75)$, where resolution focusing is almost perfect, the peak width has a resolution-limited value of ~ 1 meV full width at half maximum. The observed excitation energies and energy-integrated intensities at $(2,0,L)$ and $(3,0,L)$ ($0.1 \leq L \leq 0.85$) are plotted in Figs. 3 and 4, respectively. The closed circles represent the data from the magnetic peaks with lower excitation energy and the open circles represent the data from the ones with higher excitation energy. The solid and broken lines are the results of model calculations, which will be presented in the next section. Both at $(2,0,L)$ and $(3,0,L)$ the dispersion relations are similar and has a periodicity of 0.2 reciprocal lattice unit (r.l.u.) along the c axis which is consistent with the results by Eccleston *et al.*¹⁶ and Regnault *et al.*²⁰ Actually the dispersion relation is almost identical to the one observed in the $(0,K,L)$ zone.¹⁵ The most interesting feature is that the intensities and the ratio of the two peaks are changed with H as well as L . The intensities of the excitation peaks with lower excitation energy are more intense than those with higher excitation energy at $(2,0,L)$ ($L < 0.25$). On the other hand, the intensities of the excitation peaks with higher excitation energy are more intense than those with lower excitation energy at $(2,0,L)$ ($L > 0.6$). The intensities at $(2,0,L)$ are almost identical to those observed in the $(0,K,L)$ zone.¹⁵ The intensities at $(3,0,L)$ show com-

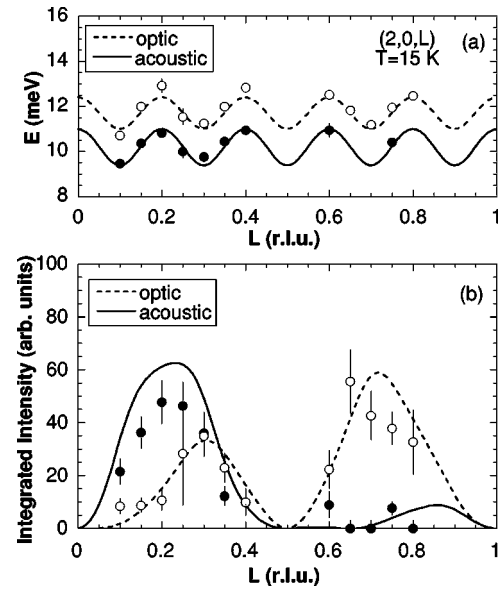


FIG. 3. Observed and calculated energies (a) and intensities (b) at $(2,0,L)$ measured at 15 K in $\text{Sr}_{14}\text{Cu}_{24}\text{O}_{41}$. The solid and broken lines, which are fits to Eqs. (2) and (3), represent the acoustic and optic modes, respectively.

pletely opposite behavior from those at $(2,0,L)$. It is noted that the intensities in Ref. 16 are the sum of intensities from the two excitations.

Figures 5 and 6 show the observed excitation energies and energy-integrated intensities at $(H,0,-0.2)$ and $(H,0,-0.7)$ ($2 \leq H \leq 4$), respectively. The closed circles represent the data from the magnetic peaks with lower excitation energy and the open circles represent the data from the ones with higher excitation energy. The solid and broken lines are the results of model calculations, which will be presented in the next section. There also exists a dispersion along the a axis with a periodicity of 2 r.l.u. The two dispersion curves along

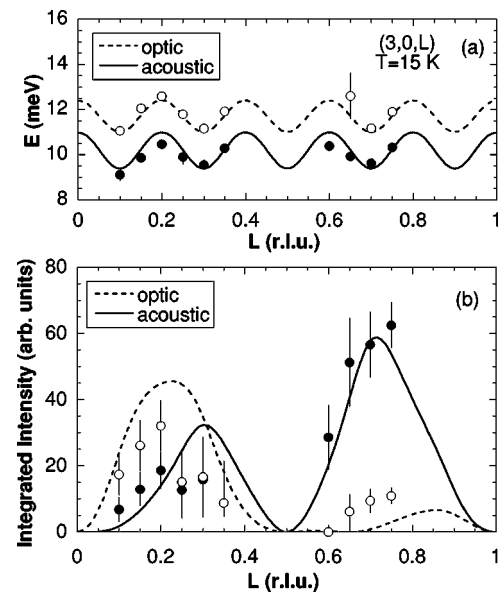


FIG. 4. Observed and calculated energies (a) and intensities (b) at $(3,0,L)$ measured at 15 K in $\text{Sr}_{14}\text{Cu}_{24}\text{O}_{41}$. The solid and broken lines, which are fits to Eqs. (2) and (3), represent the acoustic and optic modes, respectively.

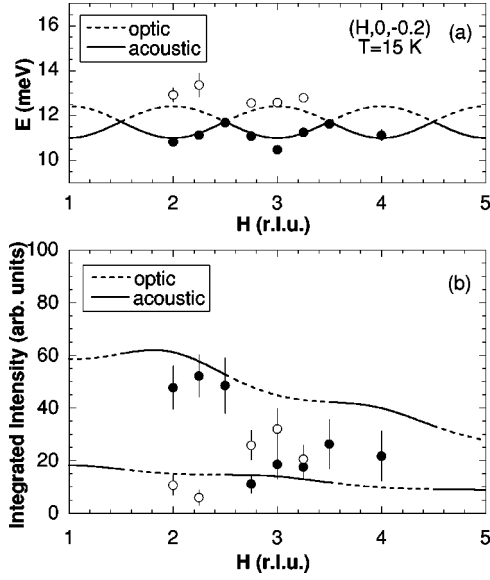


FIG. 5. Observed and calculated energies (a) and intensities (b) at $(H,0,-0.2)$ measured at 15 K in $\text{Sr}_{14}\text{Cu}_{24}\text{O}_{41}$. The solid and broken lines, which are fits to Eqs. (2) and (3), represent the acoustic and optic modes, respectively.

the a axis do not run parallel as ones along the c axis but cross at $H=\frac{5}{2}$ and $\frac{7}{2}$. The intensities of the excitation peaks with lower excitation energy are larger than those with higher excitation energy in a range of $2 < H < 2.5$ and $3.5 < H < 4$ at $(H,0,-0.2)$. On the other hand, in a range of $2.5 < H < 3.5$ the intensities of the excitation peaks with higher excitation energy are larger than those with lower excitation energy. The intensities at $(H,0,-0.7)$ show completely opposite behavior from those at $(H,0,-0.2)$. Thus, both the dispersion and the intensities depend on H and L , suggesting that there are non-negligible magnetic correlations along the a axis in addition to those along the c axis.

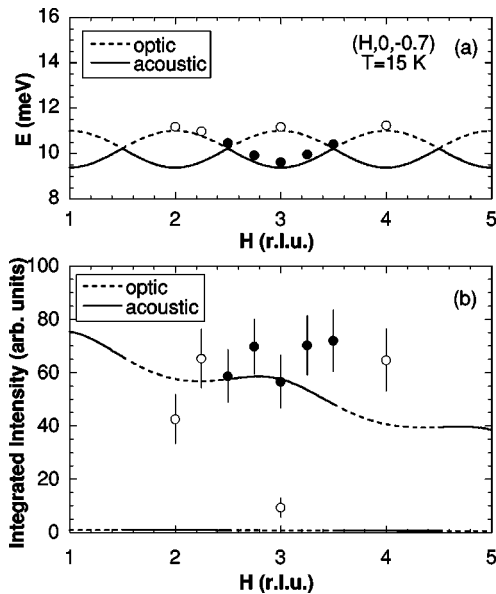


FIG. 6. Observed and calculated energies (a) and intensities (b) at $(H,0,-0.7)$ measured at 15 K in $\text{Sr}_{14}\text{Cu}_{24}\text{O}_{41}$. The solid and broken lines, which are fits to Eqs. (2) and (3), represent the acoustic and optic modes, respectively.

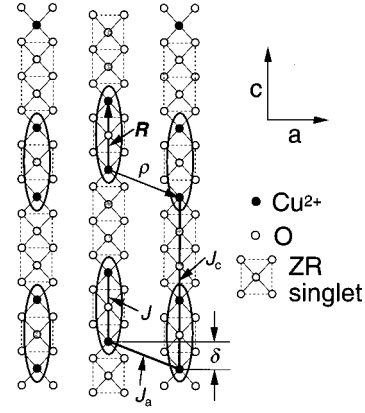


FIG. 7. A proposed model for the dimerized state and the ordering of Cu^{2+} and a ZR singlet in the ac plane.

2. Model Hamiltonian

In order to analyze the observed dispersion relation and energy-integrated intensities we used a model Hamiltonian for the dimers that are formed between Cu^{2+} spins separated by twice the distance between nearest-neighbor Cu ions and are weakly coupled along the a and c axes as shown in Fig. 7. The Hamiltonian involves three Heisenberg Hamiltonians with intradimer coupling J , interdimer coupling in the same chain J_c , and interdimer coupling between the adjacent chains J_a :

$$\hat{H} = J \sum_{\langle i,j \rangle} \mathbf{S}_i \cdot \mathbf{S}_j + J_c \sum_{\langle i,j \rangle'} \mathbf{S}_i \cdot \mathbf{S}_j + J_a \sum_{\langle i,j \rangle''} \mathbf{S}_i \cdot \mathbf{S}_j. \quad (1)$$

Here, $\langle i,j \rangle$ is nearest-neighbor spins, which are separated by twice the distance between nearest-neighbor Cu ions, in the same chain. $\langle i,j \rangle'$ is third-nearest-neighbor spins, which are separated by five times the distance between nearest-neighbor Cu ions, in the same chain. $\langle i,j \rangle''$ is nearest-neighbor spins between the adjacent chains. This model Hamiltonian is the simplest to describe the weakly coupled dimer system. As shown in Ref. 27, the Hamiltonian described in Eq. (1) is then rewritten as a Hamiltonian that describes interactions between dimers. The couplings in Eq. (1) are chosen so that they adequately describe couplings between dimers. Especially, the interdimer coupling along the c axis is for two spins separated by five times the distance between nearest-neighbor Cu ions, which explains the five times periodicity in the dispersion along the c axis.³⁰

The weakly coupled dimer system can be well described with RPA. In fact, the magnetic excitations in $\text{Cs}_3\text{Cr}_2\text{Br}_9$ (Ref. 27) and $\text{BaCuSi}_2\text{O}_6$ (Ref. 31) are successfully described with RPA treatment. The dispersion relation is given by²⁷

$$\omega^{\text{acoustic/optic}}(\mathbf{q}) = \{J^2 + J \cdot R(T) [J_c \gamma_c(\mathbf{q}) \pm J_a |\gamma_a(\mathbf{q})|]\}^{1/2},$$

$$R(T) = n_0 - n_1 = \frac{1 - \exp(-J/T)}{1 + 3 \exp(-J/T)}, \quad \gamma_c(\mathbf{q}) = 2 \cos(2\pi L),$$

$$\gamma_a(\mathbf{q}) = 2 \cos(\pi H) \cdot \exp(i2\pi L \delta), \quad (2)$$

where n_0 , n_1 , and δ are thermal populations of the singlet ground state and of the first excited triplet and the c compo-

ment of the distance between nearest-neighbor spins at the adjacent chains as shown in Fig. 7. The solid and broken lines in Figs. 3(a), 4(a), 5(a), and 6(a) represent the calculated dispersion relation of the acoustic and optic modes, respectively. Equation (2) with $J=11$ meV, $J_a=0.75$ meV, and $J_c=0.75$ meV reproduces the observed data remarkably well. In this dispersion relation, the averaged excitation energy, the bandwidth of each excitation mode, and the energy difference between the acoustic and optic modes almost correspond to J , $2J_c$, and $2J_a$, respectively. J obtained in this experiment is consistent with that obtained by Eccleston *et al.*¹⁶ The sign of J_a is consistent with that in $\text{La}_{14-x}\text{Ca}_x\text{Cu}_{24}\text{O}_{41}$ that shows a long-range magnetic ordering.^{32,33} Since the definition of the interdimer coupling along the c axis (J_c) is different from that in Ref. 16 (J_2),³⁰ the antiferromagnetic J_c is consistent with the ferromagnetic J_2 . As mentioned above, the bandwidth of each excitation mode is similar to $2J_c$ ($=1.5$ meV), which corresponds to the bandwidth $\sim J_2$ ($=1.1$ meV) in Ref. 16.

RPA treatment gives the dynamic structure factor²⁷ as the following.

$$S(\mathbf{Q}, \omega) \propto F^2(\mathbf{Q}) \cdot R(T) \cdot J \cdot [1 - \cos(\mathbf{Q} \cdot \mathbf{R})] \\ \times \left[[1 + \cos(\boldsymbol{\rho} \cdot \boldsymbol{\tau} + \phi)] \frac{1}{\omega_{\text{acoustic}}(\mathbf{q})} \right. \\ \times \delta(\omega - \omega_{\text{acoustic}}(\mathbf{q})) \\ \left. + [1 - \cos(\boldsymbol{\rho} \cdot \boldsymbol{\tau} + \phi)] \frac{1}{\omega_{\text{optic}}(\mathbf{q})} \delta(\omega - \omega_{\text{optic}}(\mathbf{q})) \right], \quad (3)$$

where $\phi = 2\pi L\delta$, $\mathbf{Q} = \mathbf{q} + \boldsymbol{\tau}$ ($\boldsymbol{\tau}$ is a reciprocal wave vector), \mathbf{R} is the vector connecting individual spins within a dimer, and $\boldsymbol{\rho}$ is a vector connecting the two sublattices, namely, the two nearest-neighbor Cu^{2+} spins between the adjacent chains. \mathbf{R} and $\boldsymbol{\rho}$ are shown in Fig. 7. The factor $[1 - \cos(\mathbf{Q} \cdot \mathbf{R})]$ can be seen in the structure factor for isolated dimers. The acoustic and optic modes can be distinguished by the factor $[1 \pm \cos(\boldsymbol{\rho} \cdot \boldsymbol{\tau} + \phi)]$. The solid and broken lines in Figs. 3(b), 4(b), 5(b), and 6(b) represent the energy-integrated intensities of the acoustic and optic modes calculated using Eq. (3), respectively. J , J_a , and J_c are fixed at the values mentioned above. δ is fixed at 0.77, which was determined by x-ray measurements at 50 K.¹⁸ Only adjustable parameter is the scale factor. The same scale factor was used for the intensities at $(2,0,L)$, $(3,0,L)$, $(H,0,-0.2)$, and $(H,0,-0.7)$. The energy-integrated intensities are described with the RPA theory reasonably well.

3. Temperature dependence

Figure 8 shows constant- Q scans at $(2,0,-0.1)$ and $(2,0,-0.6)$ as a function of temperature. The solid lines are the fits to two Gaussians. In the fitting the higher excitation energy at $(2,0,-0.1)$ and the lower excitation energy at $(2,0,-0.6)$ are fixed, which is confirmed with more intense excitation peaks at $(3,0,-0.1)$ and $(3,0,-0.6)$. It was assumed that the peak width and the intensity ratio of the two excitations are temperature independent. Temperature depen-

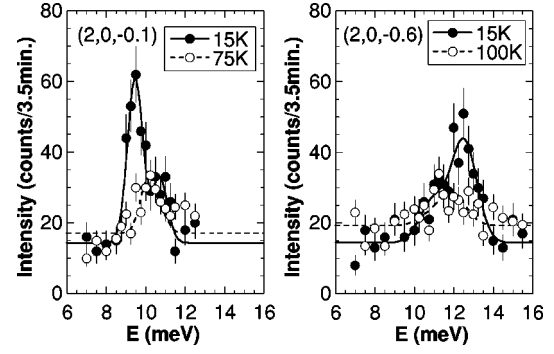


FIG. 8. Inelastic neutron spectra at $(2,0,-0.1)$ ($T=15$ and 75 K) and $(2,0,-0.6)$ ($T=15$ and 100 K) in $\text{Sr}_{14}\text{Cu}_{24}\text{O}_{41}$. The solid and broken lines are the results of fits to two Gaussians.

dence of excitation energies and energy-integrated intensities are plotted in Fig. 9. The lower excitation energy at $(2,0,-0.1)$ becomes higher and the higher excitation energy at $(2,0,-0.6)$ becomes lower with increasing temperature. Furthermore, the intensities decrease with increasing temperature. Since there is a thermal factor $R(T)$ in Eqs. (2) and (3), the RPA calculation predicts the temperature dependence of the dispersion relation and the energy-integrated intensities. The dispersion becomes flatter with increasing temperature as shown in the inset of Fig. 9 because the interdimer couplings become negligible due to large thermal fluctuations and the dimers behave like isolated dimers. The intensity is proportional to $R(T)$, which decreases with increasing temperature. The solid lines in Fig. 9 are the results of calculations using Eqs. (2) and (3). All the parameters J , J_a , J_c , δ , and scale factor are fixed at the values as determined above. The temperature dependences are fitted with the RPA calculation reasonably well although the observed intensity de-

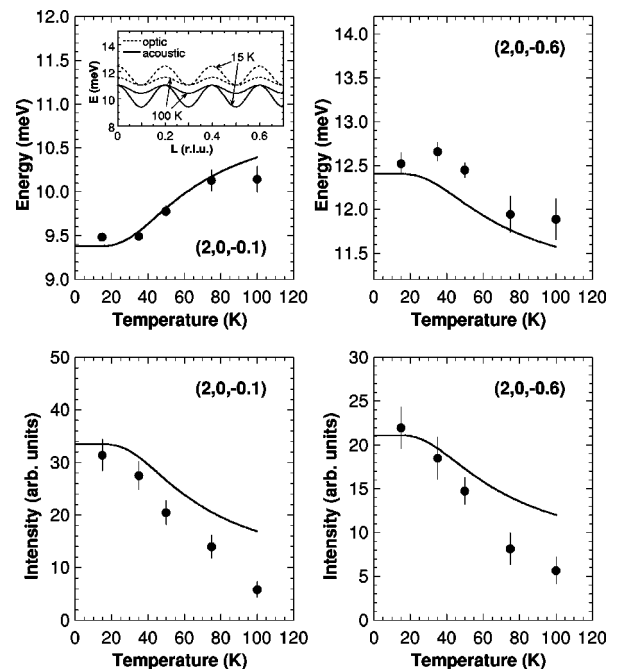


FIG. 9. Temperature dependence of the energy-integrated intensity and energy of the gap excitations at $(2,0,-0.1)$ and $(2,0,-0.6)$ in $\text{Sr}_{14}\text{Cu}_{24}\text{O}_{41}$. The solid lines are fits to Eqs. (2) and (3). The inset shows the calculated dispersion at 15 and 100 K.

creases more quickly than the calculated intensity does. This indicates that other factors in addition to thermal fluctuations disturb the dimers and the ordering of Cu^{2+} and ZR singlet. A gradual destruction of the ordering with increasing temperature suggested by NMR (Ref. 5) and x-ray measurements¹⁸ might cause the behavior.

4. Discussion

Now we discuss the relation between magnetic dimerization and structural distortion. As mentioned in Sec. I, Cox *et al.*¹⁸ performed synchrotron x-ray measurements on $\text{Sr}_{14}\text{Cu}_{24}\text{O}_{41}$ and observed superlattice Bragg peaks at $(0,0,l/4)$ and $(0,0,l/2)$ that originate from a structural distortion in the chain. This lattice distortion is probably related with the NMR results^{5,17} since the superlattice intensity also decreases gradually with increasing temperature. It should be pointed out that the x-ray experiments properly detected the coupling along the a axis but there is some disagreement along the c axis. As mentioned above, the structural distortion has correlations with two and four times periodicities along the c axis although magnetic dimers have correlations with five times periodicity. A discrepancy between magnetic and structural correlations was also reported in the spin-Peierls state in CuGeO_3 .³⁴ The magnetic excitations have a minimum energy at $(0,1,\frac{1}{2})$ but a superlattice reflection at $(\frac{1}{2},1,\frac{1}{2})$. An important point is that the x-ray results are for the ground state and neutron results are for the excited state.

We have shown that the dimer model shown in Fig. 7 explains the magnetic excitations reasonably well. The dimerized state is ascribed to the ordering of Cu^{2+} and a ZR singlet that originates from an ordering of the localized holes. Hole ordering or charge ordering occurs in various $3d$ transition-metal oxides. A quasi-two-dimensional hole ordering of the doped holes was reported in $\text{La}_2\text{NiO}_{4+\delta}$ (Ref. 35) and $\text{La}_{2-x-y}\text{Nd}_x\text{Sr}_y\text{CuO}_4$.³⁶ In the phase a static ordering of antiferromagnetic stripe is separated by charge-ordered domain walls. In the latter compound the ordered phase can be described as a stripe ordering of Cu^{2+} and ZR singlet. Manganese oxides, for example, $\text{La}_{1-x}\text{Ca}_x\text{MnO}_3$, also show a charge ordering of Mn^{3+} and Mn^{4+} .³⁷ In this system spin, charge, and orbital³⁸ degrees of freedom are closely related, which results in interesting phenomena such as colossal magnetoresistance.³⁹ NaV_2O_5 , which consists of two-leg ladders of vanadium ions, has been studied extensively since it shows a singlet ground state below 34 K.⁴⁰ The phase transition was first considered to be a conventional spin-Peierls transition.⁴¹ But the detailed inelastic neutron-scattering experiment using a single-crystal sample revealed that the magnetic excitations in the dimerized phase could not be understood by a simple one-dimensional dimerized model.⁴² NMR experiment also indicated a charge ordering of V^{4+} and V^{5+} at the transition.⁴³ Stimulated by these experimental findings, new approaches to understand the origin of the phase transition have been made theoretically.^{44,45} It is claimed that the transition is indeed closely related with a charge ordering of V^{4+} and V^{5+} ions. These various properties suggest that an intimate connection between hole/charge ordering and magnetic ordering is a common feature in the strongly correlated $3d$ transition-metal oxides. Theo-

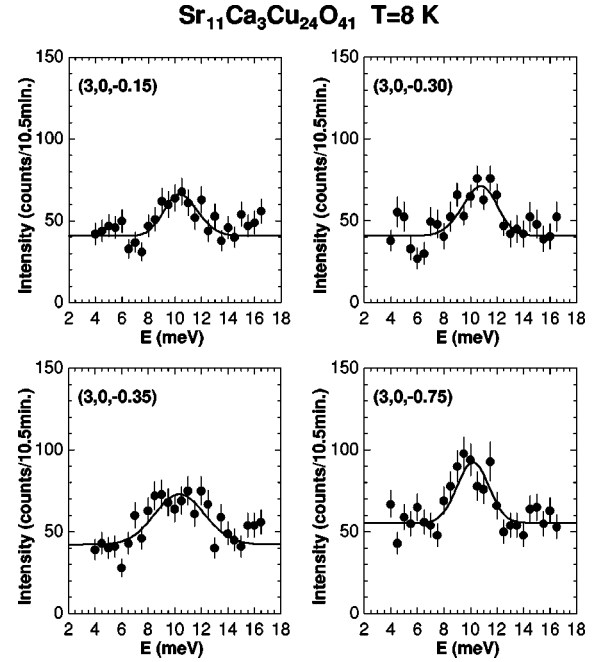


FIG. 10. Typical inelastic neutron spectra at $(3,0,L)$ at 8 K in $\text{Sr}_{11}\text{Ca}_3\text{Cu}_{24}\text{O}_{41}$. The solid lines are the results of fits to a single Gaussian or two Gaussians.

retical studies to explain the hole ordering and the dimerized state in $\text{Sr}_{14}\text{Cu}_{24}\text{O}_{41}$ are highly desirable.

B. Substitution effect in $\text{Sr}_{14-x}\text{Ca}_x\text{Cu}_{24}\text{O}_{41}$ ($x=3$)

We have also studied the substitution effect on the dimerized state. The dimerized state in the chain is most stable in pure $\text{Sr}_{14}\text{Cu}_{24}\text{O}_{41}$. When Y is substituted for Sr, the number of the holes is decreased and the number of the Cu^{2+} spins is increased. It was reported that Y substitution makes the magnetic excitation peaks broader.²⁹ As mentioned in Sec. I, the Ca substitution for Sr also reduces the number of the holes in the chain gradually.⁹⁻¹¹ Therefore, the Ca substitution is expected to affect the dimerized state in the chain.

Figure 10 shows typical inelastic neutron spectra at $(3,0,L)$ measured at 8 K in $\text{Sr}_{11}\text{Ca}_3\text{Cu}_{24}\text{O}_{41}$. The magnetic excitation peaks become broader with Ca substitution, which is similar to the case of Y substitution.²⁹ It is noted that two excitation branches are hardly resolved. However, the excitation energies are similar to those in $\text{Sr}_{14}\text{Cu}_{24}\text{O}_{41}$. The solid lines at $(3,0,-0.15)$, $(3,0,-0.30)$, and $(3,0,-0.35)$ are fits to two Gaussians and that at $(3,0,-0.75)$ is a fit to a single Gaussian by assuming that the dispersion relation is the same as that in $\text{Sr}_{14}\text{Cu}_{24}\text{O}_{41}$. The spectra are reasonably described with the simple model. As mentioned in Sec. III A, the averaged excitation energy, the bandwidth of each excitation mode, and the energy difference between the acoustic and optic modes almost correspond to J , $2J_c$, and $2J_a$, respectively. This indicates that the coupling constants J , J_c , and J_a are almost unchanged with Ca substitution although the dimerized state becomes unstable. This behavior would be explained as follows. The hole ordering sensitively depends on the hole number. Accordingly, the long-range dimer formation becomes disturbed with Ca or Y substitution.

In $\text{Sr}_{14-x}\text{Y}_x\text{Cu}_{24}\text{O}_{41}$ system, magnetic excitations are remarkably affected with Y substitution.^{15,29} In the $x=0.25$

sample the excitation peaks become broader although the dispersion relation is almost unchanged. This result suggests that J , J_c , and J_a are almost unchanged although the hole ordering is disturbed with a small amount of Y. In the $x = 1$ sample the excitation peaks become much broader, suggesting that the hole ordering becomes more unstable. An interesting behavior is that the averaged energy of the two excitations becomes reduced to ~ 9 meV, indicating that J is decreased in $\text{Sr}_{13}\text{Y}_1\text{Cu}_{24}\text{O}_{41}$. The changes of the bandwidth of each excited state, the difference in energy between two excited states, and the periodicity of the dispersion relation are difficult to determine because the peaks are too broad to be resolved as two excitations. A puzzling feature is that J is decreased in $\text{Sr}_{13}\text{Y}_1\text{Cu}_{24}\text{O}_{41}$ although the lattice constant c , which affects the exchange constant, is almost independent of Y concentration.⁴⁶

When the holes are removed further, the hole ordering cannot be observed anymore and a long-range magnetic ordering appears.^{32,33,47} The CuO_2 chains in the hole-removed $\text{Sr}_{14}\text{Cu}_{24}\text{O}_{41}$ can be considered as ferromagnetic spin chains that weakly interact with antiferromagnetic interchain coupling along the a and b axes.

In conclusion, neutron-scattering experiments have been performed on $\text{Sr}_{14}\text{Cu}_{24}\text{O}_{41}$ in order to study the dimerized state in the CuO_2 chains. The ω - Q dispersion relation as well

as the integrated intensities can be reasonably described by RPA calculation with $J = 11$ meV, $J_c = 0.75$ meV, and $J_a = 0.75$ meV. The dimer configuration indicates a quasi-two-dimensional hole ordering, which results in an ordering of magnetic Cu^{2+} with $S = \frac{1}{2}$ and a nonmagnetic ZR singlet. The hole ordering and the dimerized state are most stable in $\text{Sr}_{14}\text{Cu}_{24}\text{O}_{41}$. The Ca substitution for Sr sites makes the excitation peak broader probably because the hole ordering becomes unstable and the long-range dimer formation becomes disturbed.

ACKNOWLEDGMENTS

We would like to thank D. E. Cox, R. S. Eccleston, H. Eisaki, K. Katsumata, S. M. Shapiro, M. Takigawa, and A. Zheludev for stimulating discussions. This study was supported in part by the U.S.-Japan Cooperative Program on Neutron Scattering operated by the United States Department of Energy and the Japanese Ministry of Education, Science, Sports and Culture and by a Grant-in-Aid for Scientific Research from the Japanese Ministry of Education, Science, Sports and Culture. Work at Brookhaven National Laboratory was carried out under Contract No. DE-AC02-98CH10886, Division of Material Science, U.S. Department of Energy.

-
- ¹E. M. McCarron III, M. A. Subramanian, J. C. Calabrese, and R. L. Harlow, *Mater. Res. Bull.* **23**, 1355 (1988).
- ²T. Siegrist, L. F. Schneemeyer, S. A. Sunshine, J. V. Waszczak, and R. S. Roth, *Mater. Res. Bull.* **23**, 1429 (1988).
- ³R. S. Eccleston, M. Azuma, and M. Takano, *Phys. Rev. B* **53**, R14 721 (1996).
- ⁴K. Kumagai, S. Tsuji, M. Kato, and Y. Koike, *Phys. Rev. Lett.* **78**, 1992 (1997).
- ⁵M. Takigawa, N. Motoyama, H. Eisaki, and S. Uchida, *Phys. Rev. B* **57**, 1124 (1998).
- ⁶K. Magishi, S. Matsumoto, Y. Kitaoka, K. Ishida, K. Asayama, M. Uehara, T. Nagata, and J. Akimitsu, *Phys. Rev. B* **57**, 11 533 (1998).
- ⁷T. Imai, K. R. Thurber, K. M. Shen, A. W. Hunt, and F. C. Chou, *Phys. Rev. Lett.* **81**, 220 (1998).
- ⁸E. Dagotto and T. M. Rice, *Science* **271**, 618 (1996).
- ⁹M. Kato, K. Shiota, and Y. Koike, *Physica C* **258**, 284 (1996).
- ¹⁰Y. Mizuno, T. Tohyama, and S. Maekawa, *J. Phys. Soc. Jpn.* **66**, 937 (1997).
- ¹¹T. Osafune, N. Motoyama, H. Eisaki, and S. Uchida, *Phys. Rev. Lett.* **78**, 1980 (1997).
- ¹²N. Motoyama, T. Osafune, T. Kakeshita, H. Eisaki, and S. Uchida, *Phys. Rev. B* **55**, 3386 (1997).
- ¹³M. Uehara, T. Nagata, J. Akimitsu, H. Takahashi, N. Mori, and K. Kinoshita, *J. Phys. Soc. Jpn.* **65**, 2764 (1996).
- ¹⁴F. C. Zhang and T. M. Rice, *Phys. Rev. B* **37**, 3759 (1988).
- ¹⁵M. Matsuda, K. Katsumata, H. Eisaki, N. Motoyama, S. Uchida, S. M. Shapiro, and G. Shirane, *Phys. Rev. B* **54**, 12 199 (1996).
- ¹⁶R. S. Eccleston, M. Uehara, J. Akimitsu, H. Eisaki, N. Motoyama, and S. Uchida, *Phys. Rev. Lett.* **81**, 1702 (1998).
- ¹⁷Y. Kitaoka (private communication).
- ¹⁸D. E. Cox, T. Iglesias, K. Hirota, G. Shirane, M. Matsuda, N. Motoyama, H. Eisaki, and S. Uchida, *Phys. Rev. B* **57**, 10 750 (1998).
- ¹⁹Z. Hiroi, S. Amelinckx, G. Van Tendeloo, and N. Kobayashi, *Phys. Rev. B* **54**, 15 849 (1996).
- ²⁰L. P. Regnault, H. Moudden, J. P. Boucher, J. E. Lorenzo, A. Hiess, and A. Revcolevschi, *The Annual Report of the Institute Laue-Langevin*, 1997, p. 42 (unpublished).
- ²¹T. Barnes, J. Riera, and D. A. Tennant, cond-mat/9801224 (unpublished).
- ²²Y. Sasago, M. Hase, K. Uchinokura, M. Tokunaga, and N. Miura, *Phys. Rev. B* **52**, 3533 (1995).
- ²³A. Zheludev, G. Shirane, Y. Sasago, M. Hase, and K. Uchinokura, *Phys. Rev. B* **53**, 11 642 (1996).
- ²⁴D. A. Tennant, S. E. Nagler, A. W. Garrett, T. Barnes, and C. C. Torardi, *Phys. Rev. Lett.* **78**, 4998 (1997).
- ²⁵A. W. Garrett, S. E. Nagler, D. A. Tennant, B. C. Sales, and T. Barnes, *Phys. Rev. Lett.* **79**, 745 (1997).
- ²⁶The dispersion along the b axis is almost flat and the intensities along the b axis also monotonically decrease with increasing Q due to the magnetic form factor as reported in Ref. 15.
- ²⁷B. Leuenberger, A. Stebler, H. U. Güdel, A. Furrer, R. Feile, and J. K. Kjems, *Phys. Rev. B* **30**, 6300 (1984).
- ²⁸In Ref. 15 it was mentioned that the dispersion for the magnetic excitations at low Q is almost flat along the a axis. The mistake was made because the measurements were performed mostly at $H = \text{integer}$.
- ²⁹M. Matsuda, K. Katsumata, H. Eisaki, N. Motoyama, S. Uchida, T. Yokoo, S. M. Shapiro, G. Shirane, and J. L. Zarestky, *Phys. Rev. B* **56**, 14 499 (1997).
- ³⁰The definition of the coupling constant in the weakly coupled dimer model (J_c) is different from that in the alternating chain model (J_2) (Ref. 16) in which the interdimer coupling along the

- c* axis is for next-nearest-neighbor spins in the chain separated by three times the distance between nearest-neighbor Cu ions.
- ³¹Y. Sasago, K. Uchinokura, A. Zheludev, and G. Shirane, Phys. Rev. B **55**, 8357 (1997).
- ³²M. Matsuda, K. Katsumata, T. Yokoo, S. M. Shapiro, and G. Shirane, Phys. Rev. B **54**, R15 626 (1996).
- ³³M. Matsuda, K. M. Kojima, Y. J. Uemura, J. L. Zarestky, K. Nakajima, K. Kakurai, T. Yokoo, S. M. Shapiro, and G. Shirane, Phys. Rev. B **57**, 11 467 (1998).
- ³⁴K. Hirota, D. E. Cox, J. E. Lorenzo, G. Shirane, J. M. Tranquada, M. Hase, K. Uchinokura, H. Kojima, Y. Shibuya, and I. Tanaka, Phys. Rev. Lett. **73**, 736 (1994).
- ³⁵J. M. Tranquada, D. J. Buttrey, V. Sachan, and J. E. Lorenzo, Phys. Rev. Lett. **73**, 1003 (1994).
- ³⁶J. M. Tranquada, B. J. Sternlieb, J. D. Axe, Y. Nakamura, and S. Uchida, Nature (London) **375**, 561 (1995).
- ³⁷E. O. Wollan and W. C. Koehler, Phys. Rev. **100**, 545 (1955).
- ³⁸J. B. Goodenough, Phys. Rev. **100**, 564 (1955).
- ³⁹P. Schiffer, A. P. Ramirez, W. Bao, and S.-W. Cheong, Phys. Rev. Lett. **75**, 3336 (1995).
- ⁴⁰M. Isobe and Y. Ueda, J. Phys. Soc. Jpn. **65**, 1178 (1996).
- ⁴¹Y. Fujii, H. Nakao, T. Yosihama, M. Nishi, K. Nakajima, K. Kakurai, M. Isobe, Y. Ueda, and H. Sawa, J. Phys. Soc. Jpn. **66**, 326 (1997).
- ⁴²T. Yosihama, M. Nishi, K. Nakajima, K. Kakurai, Y. Fujii, M. Isobe, C. Kagami, and Y. Ueda, J. Phys. Soc. Jpn. **67**, 744 (1998).
- ⁴³T. Ohama, H. Yasuoka, M. Isobe, and Y. Ueda (unpublished).
- ⁴⁴H. Seo and H. Fukuyama, J. Phys. Soc. Jpn. **67**, 2602 (1998).
- ⁴⁵M. V. Mostovoy and D. I. Khomskii, cond-mat/9806215 (unpublished).
- ⁴⁶M. Kato, T. Adachi, and Y. Koike, Physica C **265**, 107 (1996).
- ⁴⁷S. A. Carter, B. Batlogg, R. J. Cava, J. J. Krajewski, W. F. Peck, Jr., and T. M. Rice, Phys. Rev. Lett. **77**, 1378 (1996).